Electrosprayed Polyamide Nanofiltration Membrane with Intercalated Structure for Controllable Structure Manipulation and Enhanced Separation Performance

Simin Yang[1,2], Jianqiang Wang[1,2*], Lifeng Fang[3], Haibo Lin[1], Fu Liu[1,2*] and Chuyang Y. Tang[4]

1. Key Laboratory of Marine Materials and Related Technologies, Zhejiang Key Laboratory of Marine Materials and Protective Technologies, Ningbo Institute of Materials Technology and Engineering, Chinese Academy of Sciences, Ningbo, China;

2. University of Chinese Academy of Sciences, Beijing, China;

3. Key Laboratory of Macromolecule Synthesis and Functionalization (MOE), Department of Polymer Science and Engineering, Zhejiang University, Hangzhou, China.

4. Department of Civil Engineering, The University of Hong Kong, Hong Kong, China.

*Please address correspondences to

Dr. Jianqiang Wang (wangjianqiang@nimte.ac.cn) and Prof. Fu Liu (fu.liu@nimte.ac.cn), Tel.:+86-574-86325963; Fax: +86-574-86325963;

Abstract

Intercalated structure and electrosprayed interfacial polymerization methods have recently been proposed for permeability enhancement of polyamide membranes. In this study, a Span 80 intercalated polyamide nanofiltration membrane was fabricated through electrospray for simultaneously improving the surface structure, interfacial stability and separation performance. The membrane obtained through electrosprayed interfacial polymerization (EIP) showed a water flux of 83.0 L m^{-2} h^{-1} at an applied pressure of 5.0 bar. The intercalated Span 80 severed as multifunctional layer for simultaneously lowering surface roughness (RSa value of polyamide, 7 nm), enhancing interfacial stability (better anti-backwashing ability) and separation performance (enhanced water flux and BPA rejection). The current study provides new opportunities for fabricating polyamide nanofiltration membrane with high performance by combination of EIP and reactive interlayer strategy.

Keywords: Electrospary; Polyamide nanofiltration membrane; Interfacial polymerization.

1. Introduction

Polyamide-based nanofiltration (NF) membrane extensively used for desalination and wastewater reclamation, is a promising technology for addressing the water scarcity issue [1-3]. A typical NF membrane is composed of a porous substrate and a dense separation layer commonly fabricated through interfacial polymerization between amine monomer and acyl chloride. The formed dense polyamide layer can reject various solutes including metal ions and organic contaminants with molecular weight in the range of 200-1000 Da [4]. Despite impressive progresses achieved in recent years, the challenge still remains e.g. precise structure control of polyamide layer and enhancement of the flux and rejection for organic compounds [5].

In order to improve the structure control and separation performance of polyamide based nanofiltration membrane, many strategies have been developed by tuning surface structure, surface chemistry and thickness of polyamide layer [6]. For example, thin film nanocomposite (TFN) membranes with a variety of nanoparticles incorporation (e.g., NaA zeolite, MCM-41, TiO_2, Ag, SiO_2, carbon nanotubes, graphene oxide and MOF/COFs) have been reported [7-15]. However, aggregation and ununiform dispersion of nanoparticles in polyamide layer remains as a critical challenge. Interfacial polymerization at the free oil/water interface was also reported for obtaining ultrathin and defect-free polyamide layer [16, 17]. However, the subsequent transfer of this ultrathin film is challengeable. Recently, an interlayer

incorporation strategy was proposed as a promising strategy for high performance NF membranes. NF membranes incorporating an interlayer of cadmium hydroxide nanostrands, carbon nanotubes, polydopamine, polydopamine-Ag, ZIF-8, Tannic acid/Fe^{3+}, cellulose nanocrystals or polyphenol show greatly improved water permeability [18-25]. However, the relatively complicated synthesis processes or post-removal of interlayer limited their applications. Moreover, interfacial stability between polyamide and the support layer needs to be further demonstrated.

In parallel to interlayer strategy, more recently, electrosprayed interfacial polymerization (EIP) was reported for fabricating polyamide reverse osmosis membrane by using m-phenylenediamine and trimesoyl chloride for enhanced separation performance [26-28]. In this process, surface structure, polyamide thickness and surface morphology of polyamide layer can be precisely tuned in analogy to 3D printing. Despite of the innovative method for reverse osmosis membrane fabrication, to the best of our knowledge, nanofiltration fabrication through electrosprayed interfacial polymerization has not been studied yet. The structure and chemistry control of electrosprayed nanofiltration membrane, the formation mechanism of polyamide and its separation performance is of great interest.

In this study, we fabricated a polyamide composite nanofiltration membrane with high performance through electrosprayed interfacial polymerization. A thin

polyamide separation layer (about 20 nm) coupled with a Span 80 interlayer contributed to interfacial stability, surface structure and separation performance enhancement. A layer-by-layer assembly of polyamide layer and unique reaction characteristic during electrospray was proposed and systematically studied. The electrosprayed interfacial polymerization and reactive interlayer (Span 80) strategies provide new insights for fabricating of high performance polyamide membranes.

2. Experimental section

Chemicals and Materials. Commercial polyether sulfone (PES) membrane was used as substrate and purchased from RisingSun Membrane (China) with a molecule weight cut-off of 20000. Hexane, acetone and ethanol of analytical grade were purchased from Sinopharm Chemical Reagent Co., Ltd (China). Span 80, piperazine (PIP, 99%), inorganic salts (Na_2SO_4, $MgSO_4$, $MgCl_2$ and NaCl), 1,3,5-Benzenetricarbonyl trichloride (TMC 99%) and BPA were all bought from Aladdin Industrial Corporation (China).

Electrospraying interfacial polymerization. An illustration of electrospraying interfacial polymerization was presented in Figure 1. Specifically, PIP was dissolved in deionized water with different weight concentration (0.06%, 0.12%, 0.24% and 0.48%). TMC was dissolved in hexane-acetone mixed solution (volume ratio of 4:1) in order to increase the spinnability (Figure S1). Concentration ratio between TMC

and PIP was set as 1:3. PES membrane was flushed by deionized water and wiped by dust-free paper, then fixed on rotating drum of electrospinning setup (SS-3556H, Ucalery, China) with a constant rotating rate of 80 rpm. Freshly prepared PIP/water and TMC/hexane-acetone solutions were loaded in two syringes respectively with feed rate of 1.2 mL/h. Distance between PES membrane and spinnerets was kept at 6.0 cm. Applied voltage was about 9 kV. During electrospray, the spinnerets kept horizontally moving (100 mm/min) from side to side for uniform formation of polyamide. After certain time of electrospray, the membrane was peeled off and heated at 60 ^{o}C for 10 min in an oven. Finally, the obtained membrane (denoted as EIP membrane) were stored in deionized water. EIP membrane fabricated through different electrospray time was denoted as EIP-X, where X stands for electrospray time.

For fabrication of Span 80 intercalated composite polyamide, a Span 80 interlayer was electrosprayed prior to the formation of polyamide. 10 g/L of Span 80/ethanol solution was electrosprayed on PES substrate. Electrospray details were as follows: distance between spinneret and PES membrane was 10 cm; feed rate was set as 1.0 mL/h; applied voltage was about 10-11 kV. The obtained membranes were air dried overnight before use and denote as S-PES. An illustration diagram for fabricating EIP and S-EIP membrane can be found in Figure S2.

For comparison, a polyamide NF membrane made by conventional interfacial polymerization was also prepared. Firstly, 50 mL of 0.24% PIP aqueous solution was poured on a PES substrate, which was clamped in a home-made device, and kept for 3 min. And then PIP solution was carefully removed by a rubber roller. After that, 50 mL of 0.08% TMC/hexane solution was introduced to cover the PES membrane for 2 min. After reaction, the synthesized membrane was washed by hexane and cured in 60 ^{o}C oven for 10 min. Finally, the obtained membrane (denoted as CIP membrane) was kept in deionized water.

Membrane Characterizations. Surface and cross-section morphologies of membranes were investigated by scanning electron microscopy (Hitachi S4800, FESEM) and transmission electron microscopy (Tecnai F20, TEM). Prior to SEM test, a thin layer of platinum was coated. The roughness and 3D images of membrane surfaces were measured by scanning probe microscope (Dimension 3100 Vecco) at a scan rate of 1 Hz in tapping mode. The scanning probe microscope images were analyzed by Nanoscope analysis 1.7 software. Zeta potential of prepared membranes was evaluated by the electrolyte analyzer (SurPASS Anton Paar, GmbH) with 1mM KCl solutions as electrolyte solution. Chemical composition of different membranes were tested by X-ray photoelectron spectroscopy (XPS, Shimadzu Axis Ultra Dld).

Membrane Separation Performance. Membrane flux and rejection were tested using a home-made cross-flow filtration apparatus. Effective filtration area of the cell was 6.15 cm^2. All NF membranes were filtrated at 6.0 bar for at least 2 h to stable **Membrane separation performance.** Pure water flux and rejection (1.0 g/L for salts, and 1.0 mg/L for BPA) performances of membranes were tested at 5.0 bar. All experiments were carried out at least three times and the average data were reported. For anti-backwashing evaluation experiments, membrane was firstly fixed in the cross-flow filtration apparatus upside down (polyamide layer faced spacer), and then pure water was used for filtration through this membrane at 6.0 bar for 1 h. After that pure water flux and salt rejection of the backwashed membrane was tested again as usual (polyamide layer faced feed solution). Rejection loss was the rejection difference before and after backwashing.

Membrane flux (J_w) was calculated through equation 1:

$$J_W = \frac{V}{S \times \Delta t} \quad (1)$$

where V, S and Δt presents the volume of permeate water (L), the effective area of membranes (m^2) and filtration time (h), respectively.

Removal efficiency (R) was calculated by equation 2:

$$R = \frac{C_f - C_p}{C_f} \times 100\% \quad (2)$$

where C_p and C_f are the concentration of permeate and feed solutions. Salt concentrations were tested by electrical conductivity meter (DDSJ-308F, Shanghai

leici instruments). Concentrations of BPA was detected by high performance liquid chromatography (1260, Agiilent Technologies Inc). Details about BPA analyze can be found in supporting information.

Membrane water permeability A and salt permeability B were calculated by equation 3 and 4:

$$A = \frac{J_W}{\Delta P - \Delta \pi} \quad (3)$$

$$B = \frac{J_w}{R} - J_w \quad (4)$$

where A (L m^{-2} h^{-1} bar^{-1}) is the membrane water permeability, △P is the applied pressure and △π is the osmotic pressure between feed solution and filtrate.

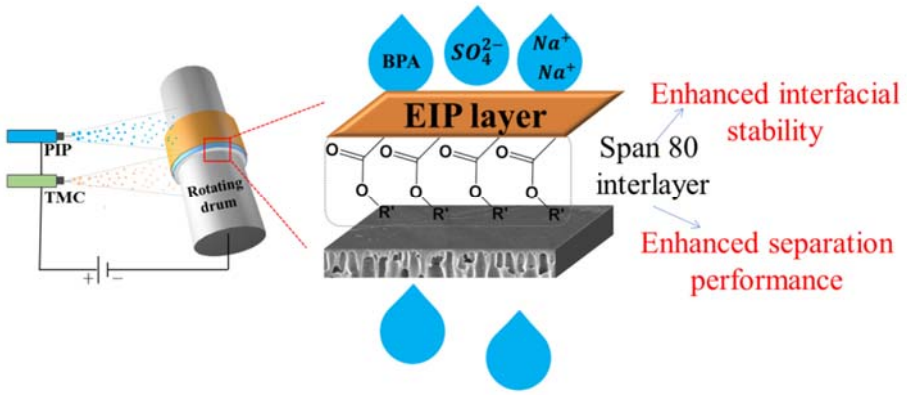

Figure1. Schematic diagram of the fabrication process and membrane characters.

3. Results and discussions

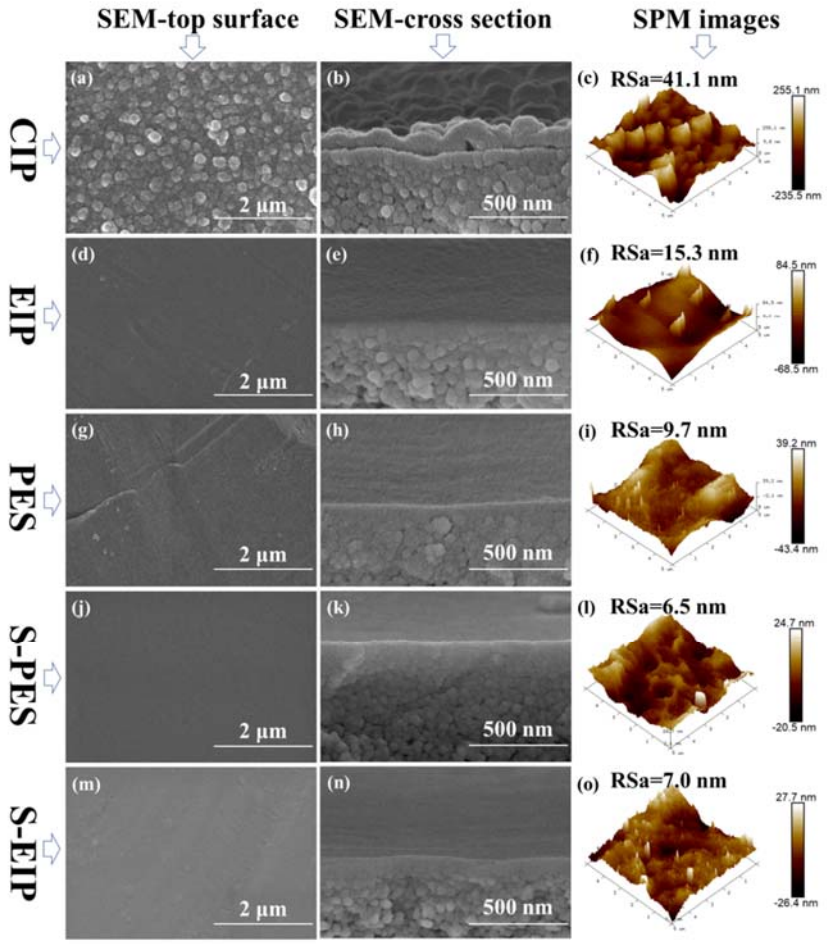

Figure 2. SEM and SPM images of different membranes, (a-c) CIP, (d-f) EIP (PIP 0.24%, TMC 0.08%), (g-i) PES substrate, (j-l) S-PES and (m-o) S-EIP (PIP 0.24%, TMC 0.12%).

Morphology and structure of membranes. Interfacial polymerization has been widely used for fabricating of polyamide based membranes and the formation mechanism became clearer now [29, 30]. However, recently reported reverse osmosis membrane prepared through electrosprayed interfacial polymerization has revolutionized the traditional understanding of polyamide formation [27, 28]. The

distinguished features of this strategy are including accurately controlled thickness and controlled surface morphologies of polyamide layer.

Different from the intrinsic bulk-reaction nature of CIP, electrosprayed interfacial polymerization simulates an additive manufacturing process with reciprocating scans of monomer spray [26, 28]. Therefore, mechanism of polyamide formation was different in EIP process compared with CIP. Figure 2a-b showed that typical "ridge-and-valley" structured polyamide layer was obtained through CIP strategy, RSa value of the membrane was 41.1 nm (Figure 2c). The roughness structure was ascribed to the localized reaction heat and escape of nanobubbles [31]. However, electrosprayed polyamide layer exhibited a relatively smooth surface (RSa = 15.3 nm, Figure 2 d-f). This roughness value was comparable to that of the PES substrate (RSa=9.7 nm, Figure 2g-i). Surface roughness can further decreased (RSa = 7.0 nm, Figure 2m-o) if a Span 80 interlayer was electrosprayed before electrosprayed interfacial polymerization. The reason was might mainly due to the flexibility of Span 80 molecular, as it contains long aliphatic tail (16 carbon atoms). The flexible Span 80 layer smoothed PES membrane, as RSa value decreased from 9.7 nm (PES, Figure 2i) to 6.5 nm (S-PES, Figure 2l). It was also not significantly affected by the PIP concentration (Figure S3). In the EIP process, polyamide was growing layer by layer with the scanning of sprayed monomer. For each scan, the interfacial polymerization was relatively isolated and facilitated the dissipation of reaction heat.

The key advantage of EIP was thickness control during polyamide formation. Compared to the relatively thick rejection layer of the CIP membrane (~ 125 nm, Figure 2b), the electrosprayed polyamide layer was quite thin, with no clear boundary between polyamide and PES substrate (Figure 2e). In addition, incorporation of an interlayer (Span 80) between polyamide and the PES substrate reduced surface roughness of both PES substrate (Figure 2j-i) and the obtained electrosprayed polyamide layer (Figure 2m-o) .

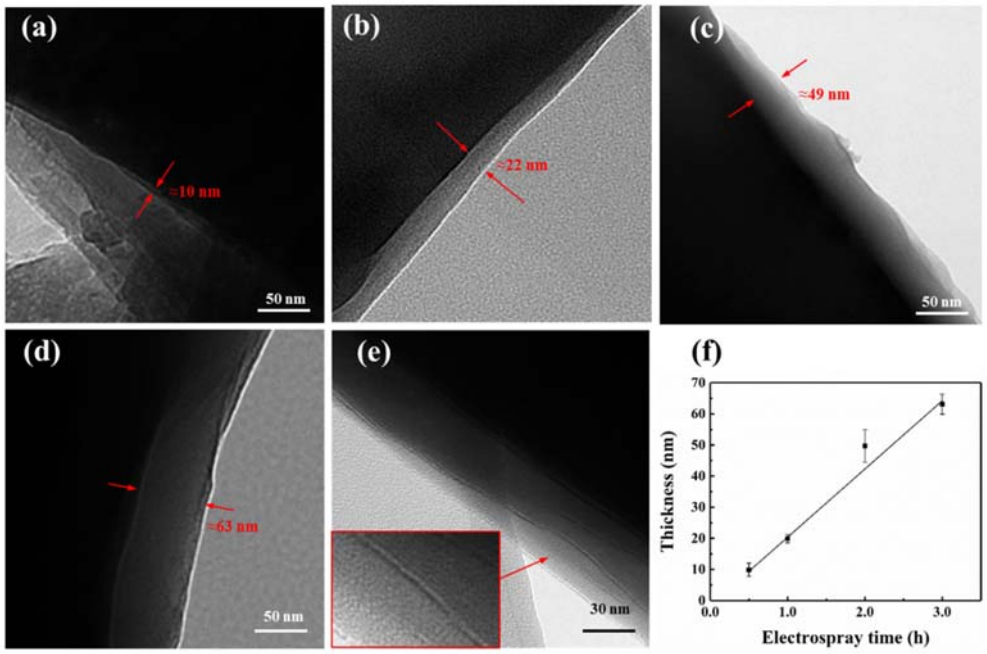

Figure 3. TEM images of different membranes: (a) EIP-0.5, (b) EIP-1, (c) EIP-2 and (d) EIP-3 (e). TEM image of electrosparyed polyamide membrane prepared by high concentration (PIP: 1.44%; TMC: 0.48%). (f) Relationship between polyamide thickness and electrospray time.

TEM was applied to explore the structure of electrosprayed polyamide layer. Results in Figure 3 showed that clear polyamide layer can be found on top of PES substrate. Thickness of electrosprayed polyamide layer increased linearly with electrospray time (Figure 3f), which can be controlled from 10 nm to 63 nm with extending spray time from 0.5 h to 3.0 h (Figure 3a-d). A growth rate of 22 nm/h (0.73 nm/scan) was obtained under current electrospray conditions.

Notably, a lamellar structure was clearly observed from the cross section of electrosprayed polyamide layer (inset image of Figure 3e), which is distinctly different from the isotropic structure of cross-linked polyamide matrix formed in CIP process. Typical lamellar spacing with low density can be found between adjacent polyamide layers, which can function as additional nano-channels for water transportation. Therefore, both significantly reduced thickness and additional water channels of EIP polyamide nanofiltration membranes could contributed enhanced flux while maintaining high rejection.

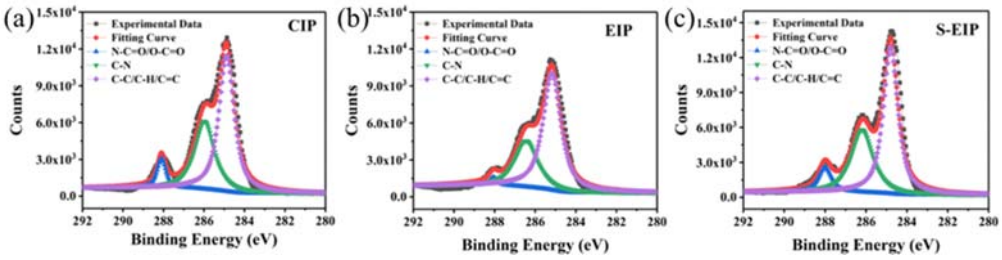

Figure 4. C 1s core level spectra of CIP (a), EIP (b) and S-EIP (c) membrane. EIP and S-EIP membranes were fabricated using 0.24% PIP and 0.08% TMC.

XPS results in Figure 4 verified the formation of amide bonds, and CIP, EIP and S-EIP membranes exhibited similar chemical structure. –O–C=O/–N–C=O peak at 288.1 eV and C–N peak at 286 eV were attributed to the typical polyamide structure, which formed from the reaction between PIP and TMC [32]. The above results confirmed that polyamide layer can be formed on the ultrafiltration substrate through both CIP and EIP strategies.

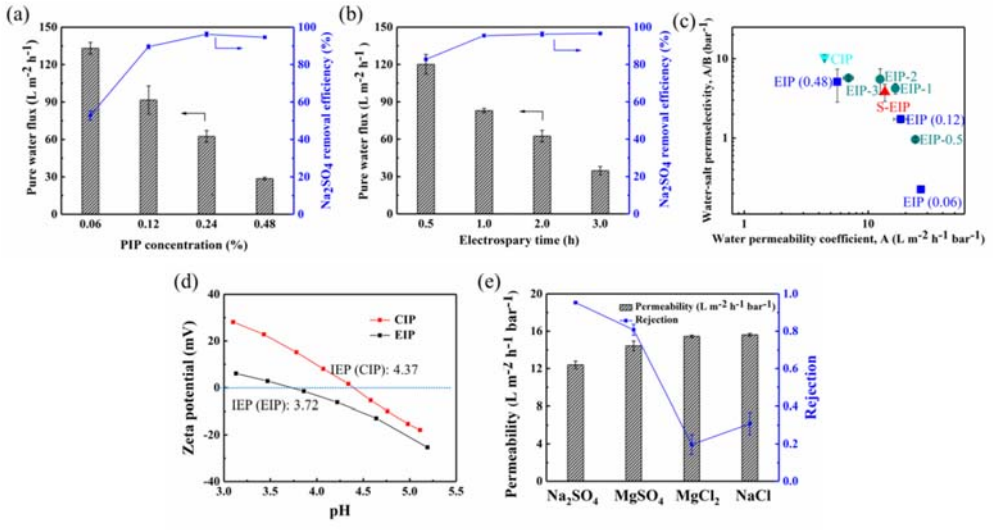

Figure 5. Flux and rejection performances of electrosprayed membranes using different PIP concentrations (a, ratio of TMC/PIP was 1:3; electrospray time was 2 h) and different electrospray time (b); water-salt permselectivity (A/B) vs. water permeability (A) of polyamide membranes (c, EIP(x), x stands for PIP concentration). Zeta potential properties of EIP, S-EIP and CIP membranes (d). Separation performance of EIP-1 and S-EIP membrane for different salts (e).

Separation performance and formation mechanism of polyamide. Figure 5a showed that PIP concentration during electrospray has a strong effect on separation performance of membrane. As PIP concentration increased from 0.06% to 0.48%, membrane flux decreased form 133.1 L m^{-2} h^{-1} to 28.6 L m^{-2} h^{-1}. Meanwhile, rejection for Na_2SO_4 of the membrane was increased from 52.9% to 96.3%. Low monomer concentration may cause a thin, loose or even incomplete polyamide layer, and ions just go through the thin film layer with defects, which weakened the membrane selectivity accordingly. These results were similar with the traditional interfacial polymerization process as PIP concentration has a great effect on the formation of selective layer and separation performance [20]. An optimal flux (62.5 L m^{-2} h^{-1}) and rejection (96.3%) was obtained when PIP concentration was 0.24%.

As thinner polyamide can offer higher flux [33], thickness of polyamide layer was tuned by electrospray time. Results in Figure 5b indicated that membrane flux gradually decreased from 120.1 L m^{-2} h^{-1} to 34.7 L m^{-2} h^{-1} as electrospray time increased from 0.5 h to 3 h. Meanwhile, rejection for Na_2SO_4 was firstly increased from 82.7% (0.5 h) to 95.5% (1 h) and then leveled off after 1 h of electrospray. Membrane with 1 h of electrospray (EIP-1) exhibited a water flux of 83.0 L m^{-2} h^{-1} which was 33.0% improvement compared with membrane with 2 h of electrospray (EIP-2). Therefore, 1 h of electrospray was considered as the optimal condition and following membrane samples were fabricated based on this condition. A comparison

of water-salt permselectivity (A/B) towards water permeability (A) was showed in Figure 5c. According to the results in Figure 5c, EIP method can precisely manipulate the water-salt permselectivity in a wide range, and endow membrane with higher A value with comparable A/B value with CIP membrane.

Separation performance of membrane fabricated in this study was compared with previous literatures reported membranes. As Table 1 showed that most of polyamide based nanofiltration membranes (including commercially available NF270 membrane) prepared with conventional interfacial polymerization exhibited a low permeability of lower than or around 10 L m^{-2} h^{-1} bar^{-1} despite the difference of amine monomer and acryl chloride monomer. However, the electrosprayed membrane (EIP-1) showed significantly higher permeability (16.6 L m^{-2} h^{-1} bar^{-1}), which was nearly four times of control CIP membrane (4.4 L m^{-2} h^{-1} bar^{-1}) and 48.2% enhancement compared with NF270 membrane. This enhancement of water permeability can be attributed to the reduction of polyamide thickness through the electrospray strategy. However, Na_2SO_4 rejection of EIP membrane was slightly decreased compared with CIP membrane. The reason might due to the slightly decreased crosslinking degree of EIP membrane as discrete interfacial polymerization through electrospray. XPS results in Figure 4 also showed slightly decreased –O–C=O/–N–C=O component in EIP.

Table 1. Comparison of different membranes.

Monomers	Na_2SO_4 rejection (%)	Pure water permeability ($L\ m^{-2}\ h^{-1}\ bar^{-1}$)	Refs
PEI/PAA	98.3	5.5	[34]
PIP/DA	98	9.8	[35]
PIP/TMC/Si	97.4	7.8	[11]
PIP/mm-BTEC	95	10.3	[36]
PIP/CS	89.1	10.1	[37]
NF90	99.1	7.0	[23]
NF270	98.5	11.2	[23]
PIP/TMC (EIP)	95.5±0.7	16.6±0.4	This work
PIP/TMC (CIP)	98.1±0.15	4.4±0.2	This work

Donnan effect associated with polyamide chemistry influenced the partitioning and transport of ions and solutes [38, 39]. In a typical CIP process, the occurrence of interfacial polymerization was commonly considered in organic phase due to limited solubility and diffusivity of TMC in water [40, 41]. However, situation was different in EIP process. Figure 1 showed that organic phase (TMC/hexane/acetone) and water phase (PIP/water) were ejected from two parallel needles with equal collection distance (6 cm). The evaporation time of a microdroplet was closely related to its surface tension, partial pressure and density etc [42]. Hexane/acetone solution was completely evaporated during electrospray under current experimental conditions

(Figure S4). However, water phase cannot be completely evaporated (Figure S4). Therefore, electrosprayed interfacial polymerization reaction was actually occurred on the interface of water rather than in organic phase, which resulted in enhanced hydrolysis of acyl chloride [43]. Zeta potential results (Figure 5d) showed that membrane fabricated through EIP strategy was more negatively charged compared with CIP strategy. Relatively low rejection of $MgSO_4$ compared with Na_2SO_4 further confirmed negatively charged property of electrosprayed polyamide membrane (Figure 5e). Rejections for $MgCl_2$ and NaCl were in the range of 20%-30% (Figure 6b).

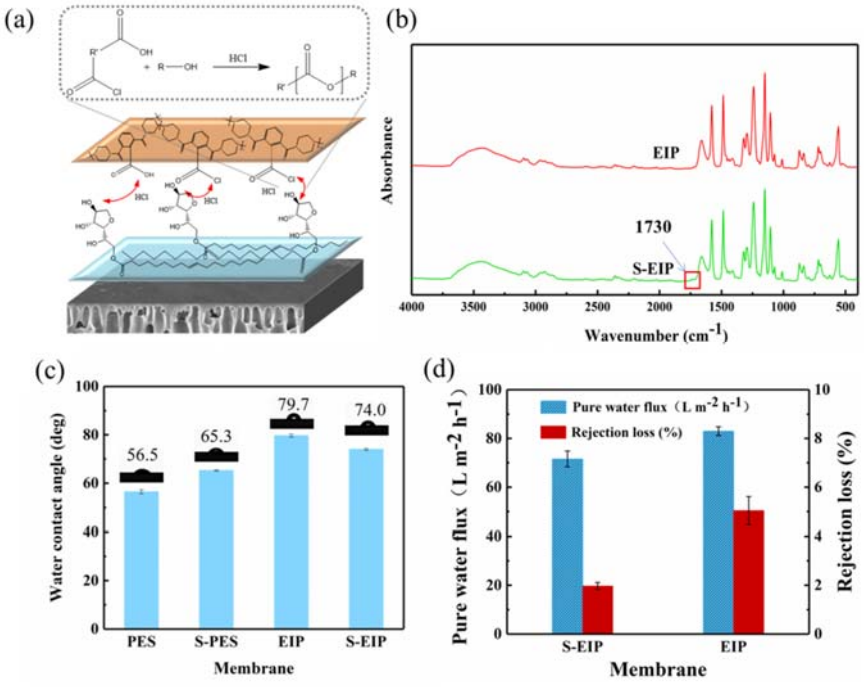

Figure 6. Illustration of reaction between Span 80 and polyamide layer (a); ATR-FTIR spectrums of EIP and S-EIP membranes (b); Water contact angle of

different membranes (c); Pure water flux and rejection loss (difference before and after backwashing at 6 bar for 1 h) of S-EIP and EIP membrane (d).

Function of Span 80 interlayer. Interlayered polyamide composite structure was recently developed for high performance nanofiltration membranes [7-13]. Permeability enhancement was commonly reported [44]. However, combination stability between polyamide layer and support layer was often decreased. In this study, a Span 80 interlayer was incorporated in electrospray process for strengthening the combination between polyamide layer and support layer. Hydroxyl groups in Span 80 covalently bonded with acyl chloride (or hydrolyzed carboxyl groups) under the catalysis of hydrogen chloride produced during interfacial polymerization (Figure 6a). The occurrence of carbonyl ester peak at 1730 cm^{-1} for S-EIP (Figure 6b) verified this reaction. Water contact angle of PES membrane increased from 56.5° to 65.3° after Span 80 electrospray, which was mainly due to the hydrophobic nature of Span 80 (Figure 6c). S-PES membrane increased the penetration resistance of water phase compared with PES membrane. Therefore, more water can be available on S-PES membrane surface in subsequent electrosprayed interfacial polymerization process, which enhanced the hydrolysis of TMC molecules. The enhanced hydrolysis of TMC endowed the S-EIP membrane with a relative small water contact angle (74.0°) compare with EIP (79.7°, Figure 6c). The aliphatic chain of Span 80 bonded with support layer through hydrophobic interactions [45]. As some TMC molecules were

consumed by Span 80, concentration of TMC was re-optimized. The S-EIP membrane exhibited membrane permeability of 13.4±0.6 L m^{-2} h^{-1} bar^{-1} (Figure S6). The backwashing results in Figure 6d indicated that pure water flux was nearly maintained, while rejection loss (for Na_2SO_4) of S-EIP was smaller than EIP membrane without Span 80 interlayer. This was mainly due to the bridging effect of Span 80 between polyamide and support layer. In addition, long-term separation performances of EIP and S-EIP membranes in Figure S7 suggested their stability.

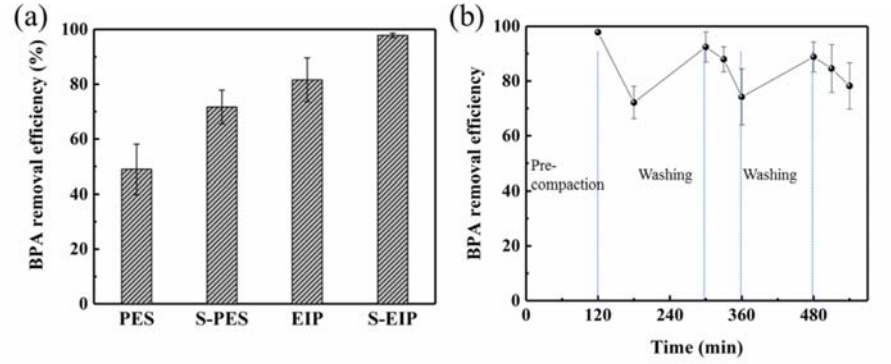

Figure 7. BPA rejection performance of different membranes (a) and recycle performance for BPA removal (b).

More interestingly, BPA rejection performances were increased after Span 80 incorporation despite of the support membrane or electrosprayed nanofiltration membrane (Figure 7a). EIP membrane without Span 80 interlayer showed BPA rejection of 81.6%, however, BPA rejection of S-EIP membrane with Span 80 interlayer was increased to 97.8%. Actually, common polyamide based nanofiltration membranes can only reject 50%-80% of BPA depends on the membrane composition

[46]. Therefore, except for the reduction of surface roughness and enhancement of interfacial stability, incorporated Span 80 can also benefit for BPA removal. The main reason for BPA removal enhancement was might due to synergistic hydrophobic interaction and hydrogen bonding attraction between Span 80 and BPA [47]. The aliphatic hydrocarbon chain served as the hydrophobic groups in Span 80, and it can easily attach with the two methyl groups in BPA due to similar solubility parameters [45, 48]. Meanwhile, hydroxyl groups in both Span 80 and BPA facilitate the hydrogen bonding between each other. In addition, BPA removal performance of S-EIP membrane can be regenerated through a simple washing using ethanol solution (Figure 7b). A comparison between the current study and previous literatures was made (Table 2). The results indicated that membrane permeability of S-EIP was more than two times of higher than some of the literatures reported membranes with comparable BPA removal efficiency.

Table 2. Preparation conditions and performance of TFC membranes.

Membrane	EDC Rejection (%)	Pure water permeability (L m^{-2} h^{-1} bar^{-1})	Refs
NF90/PDA	99 (BPA)	3.9	[46]
PIP/DA	99 (BPA)	6.3	[49]
PIP/TMC/BA	＞80	6.1	[50]
TA/Fe	99.7 (benzylparaben)	5.1	[51]
PIP/TMC/MEA	90.8	6.5	[52]
PIP/TMC(S-EIP)	97.8±0.78（BPA）	13.4±0.6	This work

4. Conclusions

In this study, we fabricated a Span 80 intercalated polyamide composite nanofiltration membrane with reduced surface roughness, enhanced flux, interfacial stability (polyamide layer and support layer) and also BPA removal ability through electrospray strategy. Electrosprayed interfacial polymerization (EIP) simulating nano-scaled additive manufacturing process, offers distinguished features including precise thickness control (several to dozens of nanometers), smoothed and negatively charged surface and lamellar structured nano-channels. Reduced thickness and additional lamellar spacing nano-channels are responsible for flux enhancement compared to conventional interfacial polymerization (CIP). In addition, in order to enhance the interfacial stability between polyamide and support layers, Span 80 interlayer was introduced. Span 80 interlayer exhibited several important features for nanofiltration membrane fabrication, including more smoothed polyamide surface, enhanced anti-backwashing ability and enhanced BPA removal efficiency. Strategy proposed in the current study may provide more opportunity for polyamide nanofiltration fabrication.

Acknowledgments

This work is financially supported by National Nature Science Foundation of China (51703233, 51973230, 5161101025), Zhejiang Provincial Natural Science Foundation of China for Distinguished Young Scholars (LR20E030002), Ten thousand plan-high

level talents special support plan of Zhejiang province, China (ZJWR0108020) and Nature Science Foundation of Ningbo (2018A610026).

Conflict of interest

The authors declare no conflict of interest.

References

[1] M. Elimelech, W.A. Phillip, The future of seawater desalination: Energy, technology, and the environment, Science, 333 (2011) 712-717.
[2] J.R. Werber, C.O. Osuji, M. Elimelech, Materials for next-generation desalination and water purification membranes, Nat. Rev. Mater., 1 (2016) 1-16.
[3] C.Y. Tang, Z. Yang, H. Guo, J.J. Wen, L.D. Nghiem, E. Cornelissen, Potable water reuse through advanced membrane technology, Environ. Sci. Technol., 52 (2018) 10215-10223.
[4] A.W. Mohammad, Y.H. Teow, W.L. Ang, Y.T. Chung, D.L. Oatley-Radcliffe, N. Hilal, Nanofiltration membranes review: Recent advances and future prospects, Desalination, 356 (2015) 226-254.
[5] Z. Yang, X.H. Ma, C.Y.Y. Tang, Recent development of novel membranes for desalination, Desalination, 434 (2018) 37-59.
[6] M. Paul, S.D. Jons, Chemistry and fabrication of polymeric nanofiltration membranes: A review, Polymer, 103 (2016) 417-456.
[7] B.-H. Jeong, E.M.V. Hoek, Y. Yan, A. Subramani, X. Huang, G. Hurwitz, A.K. Ghosh, A. Jawor, Interfacial polymerization of thin film nanocomposites: A new concept for reverse osmosis membranes, J. Membr. Sci., 294 (2007) 1-7.
[8] J. Yin, E.S. Kim, J. Yang, B.L. Deng, Fabrication of a novel thin-film nanocomposite (tfn) membrane containing mcm-41 silica nanoparticles (nps) for water purification, J. Membr. Sci., 423 (2012) 238-246.
[9] H.S. Lee, S.J. Im, J.H. Kim, H.J. Kim, J.P. Kim, B.R. Min, Polyamide thin-film nanofiltration membranes containing tio2 nanoparticles, Desalination, 219 (2008) 48-56.
[10] X. Liu, S. Qi, Y. Li, L. Yang, B. Cao, C.Y. Tang, Synthesis and characterization of novel antibacterial silver nanocomposite nanofiltration and forward osmosis membranes based on layer-by-layer assembly, Water Res., 47 (2013) 3081-3092.
[11] D. Hu, Z.L. Xu, C. Chen, Polypiperazine-amide nanofiltration membrane containing silica nanoparticles prepared by interfacial polymerization, Desalination, 301 (2012) 75-81.
[12] S. Roy, S.A. Ntim, S. Mitra, K.K. Sirkar, Facile fabrication of superior nanofiltration membranes from interfacially polymerized cnt-polymer composites, J. Membr. Sci., 375 (2011) 81-87.
[13] F. Perreault, M.E. Tousley, M. Elimelech, Thin-film composite polyamide membranes functionalized with biocidal graphene oxide nanosheets, Environ. Sci. Technol. Lett., 1 (2014) 71-76.

[14] S. Sorribas, P. Gorgojo, C. Tellez, J. Coronas, A.G. Livingston, High flux thin film nanocomposite membranes based on metal-organic frameworks for organic solvent nanofiltration, J. Am. Chem. Soc., 135 (2013) 15201-15208.
[15] C. Li, S.X. Li, L. Tian, J.M. Zhang, B.W. Su, M.Z. Hu, Covalent organic frameworks (cofs)-incorporated thin film nanocomposite (tfn) membranes for high-flux organic solvent nanofiltration (osn), J. Membr. Sci., 572 (2019) 520-531.
[16] Z.W. Jiang, S. Karan, A.G. Livingston, Water transport through ultrathin polyamide nanofilms used for reverse osmosis, Adv. Mater., 30 (2018) 1705973.
[17] J.Y. Zhu, J.W. Hou, R.J. Zhang, S.S. Yuan, J. Li, M.M. Tian, P.H. Wang, Y.T. Zhang, A. Volodin, B. Van der Bruggen, Rapid water transport through controllable, ultrathin polyamide nanofilms for high-performance nanofiltration, J. Mater. Chem. A, 6 (2018) 15701-15709.
[18] S. Karan, Z.W. Jiang, A.G. Livingston, Sub-10 nm polyamide nanofilms with ultrafast solvent transport for molecular separation, Science, 348 (2015) 1347-1351.
[19] Y.Z. Zhu, W. Xie, S.J. Gao, F. Zhang, W.B. Zhang, Z.Y. Liu, J. Jin, Single-walled carbon nanotube film supported nanofiltration membrane with a nearly 10 nm thick polyamide selective layer for high-flux and high-rejection desalination, Small, 12 (2016) 5034-5041.
[20] Y. Li, Y. Su, J. Li, X. Zhao, R. Zhang, X. Fan, J. Zhu, Y. Ma, Y. Liu, Z. Jiang, Preparation of thin film composite nanofiltration membrane with improved structural stability through the mediation of polydopamine, J. Membr. Sci., 476 (2015) 10-19.
[21] Z. Yang, Y. Wu, H. Guo, X.-H. Ma, C.-E. Lin, Y. Zhou, B. Cao, B.-K. Zhu, K. Shih, C.Y. Tang, A novel thin-film nano-templated composite membrane with in situ silver nanoparticles loading: Separation performance enhancement and implications, J. Membr. Sci., 544 (2017) 351-358.
[22] Z.Y. Wang, Z.X. Wang, S.H. Lin, H.L. Jin, S.J. Gao, Y.Z. Zhu, J. Jin, Nanoparticle-templated nanofiltration membranes for ultrahigh performance desalination, Nat. Commun., 9 (2018).
[23] Z. Yang, Z.W. Zhou, H. Guo, Z.K. Yao, X.H. Ma, X.X. Song, S.P. Feng, C.Y.Y. Tang, Tannic acid/fe3+ nanoscaffold for interfacial polymerization: Toward enhanced nanofiltration performance, Environ. Sci. Technol., 52 (2018) 9341-9349.
[24] J.J. Wang, H.C. Yang, M.B. Wu, X. Zhang, Z.K. Xu, Nanofiltration membranes with cellulose nanocrystals as an interlayer for unprecedented performance, J. Mater. Chem. A, 6 (2018) 16274-16274.
[25] X. Zhang, Y. Lv, H.C. Yang, Y. Du, Z.K. Xu, Polyphenol coating as an interlayer for thin-film composite membranes with enhanced nanofiltration performance, ACS Appl. Mater. Interfaces, 8 (2016) 32512-32519.
[26] L.L. Shan, J.H. Gu, H.W. Fan, S.L. Ji, G.J. Zhang, Microphase diffusion-controlled interfacial polymerization for an ultrahigh permeability nanofiltration membrane, ACS Appl. Mater. Interfaces, 9 (2017) 44820-44827.
[27] X.-H. Ma, Z. Yang, Z.-K. Yao, H. Guo, Z.-L. Xu, C.Y. Tang, Interfacial polymerization with electrosprayed microdroplets: Toward controllable and ultrathin polyamide membranes, Environ. Sci. Technol. Lett., 5 (2018) 117-122.
[28] M.R. Chowdhury, J. Steffes, B.D. Huey, J.R. McCutcheon, 3d printed polyamide membranes for desalination, Science, 361 (2018) 682-685.
[29] W.J. Lau, S. Gray, T. Matsuura, D. Emadzadeh, J. Paul Chen, A.F. Ismail, A review on polyamide

thin film nanocomposite (tfn) membranes: History, applications, challenges and approaches, Water Res., 80 (2015) 306-324.
[30] Y. Song, P. Sun, L. Henry, B. Sun, Mechanisms of structure and performance controlled thin film composite membrane formation via interfacial polymerization process, J. Membr. Sci., 251 (2005) 67-79.
[31] X.H. Ma, Z.K. Yao, Z. Yang, H. Guo, Z.L. Xu, C.Y.Y. Tang, M. Elimelech, Nanofoaming of polyamide desalination membranes to tune permeability and selectivity, Environ. Sci. Technol. Lett., 5 (2018) 123-130.
[32] Y.S. Jinming Peng, Wenjuan Chen, Xueting Zhao, ZhongyiJiang, Yanan Dong, Yan Zhang, Jiazhen Liu, Xingzhong Cao, Polyamide nanofiltration membrane with high separation performance prepared by edc/nhs mediated interfacial polymerization, J. Membr. Sci., 427 (2013) 92-100.
[33] B. Van der Bruggen, C. Vandecasteele, Flux decline during nanofiltration of organic components in aqueous solution, Environ. Sci. Technol., 35 (2001) 3535-3540.
[34] Y.L. Chen, F. Liu, Y. Wang, H.B. Lin, L. Han, A tight nanofiltration membrane with multi-charged nanofilms for high rejection to concentrated salts, J. Membr. Sci., 537 (2017) 407-415.
[35] M.B.M.Y. Ang, Y.L. Ji, S.H. Huang, K.R. Lee, J.Y. Lai, A facile and versatile strategy for fabricating thin-film nanocomposite membranes with polydopamine-piperazine nanoparticles generated in situ, J. Membr. Sci., 579 (2019) 79-89.
[36] L. Li, S.B. Zhang, X.S. Zhang, Preparation and characterization of poly(piperazineamide) composite nanofiltration membrane by interfacial polymerization of 3,3 ',5,5 '-biphenyl tetraacyl chloride and piperazine, J. Membr. Sci., 335 (2009) 133-139.
[37] Y.J. Tang, L.J. Wang, Z.L. Xu, H.Z. Zhang, Novel chitosan-piperazine composite nanofiltration membranes for the desalination of brackish water and seawater, J. Polym. Res., 25 (2018).
[38] R. Levenstein, D. Hasson, R. Semiat, Utilization of the donnan effect for improving electrolyte separation with nanofiltration membranes, J. Membr. Sci., 116 (1996) 77-92.
[39] J. Schaep, B. Van der Bruggen, C. Vandecasteele, D. Wilms, Influence of ion size and charge in nanofiltration, Sep. Purif. Technol., 14 (1998) 155-162.
[40] V. Percec, Interfacial polycondensation .1. And interfacial polycondensation .2. Fundamentals of polymer formation at liquid interfaces - comments, J. Polym. Sci., Part A: Polym. Chem., 34 (1996) 531-559.
[41] V. Freger, Kinetics of film formation by interfacial polycondensation, Langmuir, 21 (2005) 1884-1894.
[42] J. Wang, X. Pei, G. Liu, Q. Han, S. Yang, F. Liu, "Living" electrospray - a controllable polydopamine nano-coating strategy with zero liquid discharge for separation, J. Membr. Sci., 586 (2019) 170-176.
[43] A.K. Ghosh, B.H. Jeong, X.F. Huang, E.M.V. Hoek, Impacts of reaction and curing conditions on polyamide composite reverse osmosis membrane properties, J. Membr. Sci., 311 (2008) 34-45.
[44] R.J. Zhang, S.L. Yu, W.X. Shi, J.Y. Zhu, B. Van der Bruggen, Support membrane pore blockage (smpb): An important phenomenon during the fabrication of thin film composite membrane via interfacial polymerization, Sep. Purif. Technol., 215 (2019) 670-680.

[45] Y. Ding, J. Wu, J. Wang, H. Lin, J. Wang, G. Liu, X. Pei, F. Liu, C.Y. Tang, Superhydrophilic and mechanical robust pvdf nanofibrous membrane through facile interfacial span 80 welding for excellent oil/water separation, Appl. Surf. Sci., 485 (2019) 179-187.
[46] H. Guo, Y. Deng, Z. Tao, Z. Yao, J. Wang, C. Lin, T. Zhang, B. Zhu, C.Y. Tang, Does hydrophilic polydopamine coating enhance membrane rejection of hydrophobic endocrine-disrupting compounds?, Environ. Sci. Technol. Lett., 3 (2016) 332-338.
[47] Y.W. Zhu, J.F. Wei, H. Zhang, K. Liu, Z.Y. Kong, Y. Dong, G. Jin, J. Tian, Z. Qin, Fabrication of composite membrane with adsorption property and its application to the removal of endocrine disrupting compounds during filtration process, Chem. Eng. J., 352 (2018) 53-63.
[48] J.L. Acero, F.J. Benitez, F.J. Real, F. Teva, Removal of emerging contaminants from secondary effluents by micellar-enhanced ultrafiltration, Sep. Purif. Technol., 181 (2017) 123-131.
[49] H. Guo, Y. Deng, Z. Yao, Z. Yang, J. Wang, C. Lin, T. Zhang, B. Zhu, C.Y. Tang, A highly selective surface coating for enhanced membrane rejection of endocrine disrupting compounds: Mechanistic insights and implications, Water Res., 121 (2017) 197-203.
[50] Y.-l. Liu, X.-m. Wang, H.-w. Yang, Y.F. Xie, X. Huang, Preparation of nanofiltration membranes for high rejection of organic micropollutants and low rejection of divalent cations, J. Membr. Sci., 572 (2019) 152-160.
[51] H. Guo, L.E. Peng, Z.K. Yao, Z. Yang, X.H. Ma, C.Y.Y. Tang, Non-polyamide based nanofiltration membranes using green metal-organic coordination complexes: Implications for the removal of trace organic contaminants, Environ. Sci. Technol., 53 (2019) 2688-2694.
[52] Y.-l. Liu, Y.-y. Zhao, X.-m. Wang, X.-h. Wen, X. Huang, Y.F. Xie, Effect of varying piperazine concentration and post-modification on prepared nanofiltration membranes in selectively rejecting organic micropollutants and salts, J. Membr. Sci., 582 (2019) 274-283.